High-Pressure Chemistry

DOI: 10.1002/ange.201108713

Hypervalent Octahedral SiH_6^{2-} Species from High-Pressure Synthesis**

*Kati Puhakainen, Daryn Benson, Johanna Nylén, Sumit Konar, Emil Stoyanov, Kurt Leinenweber, and Ulrich Häussermann**

Hypervalence is a well established concept in chemistry, referring to aggregates (molecules, ions, extended structures) in which main group atoms—through their coordination with ligands—attain an environment of electron pairs that exceeds the number of four.[1] The phenomenon is typically associated with sufficiently large central atoms (from periods 3 and higher) and electronegative ligands, such as F, Cl, and O. Bonding in hypervalent species is conveniently described by the three-electron, four-center (3c4e) model[2] and it is commonly believed that a high polarity is essential for stabilizing the hypervalent bond.[3]

The electronegativity of hydrogen is similar to p element central atoms, and this is one of the reasons why hydrogen is rarely observed as ligand in hypervalent species. With phosphorus the neutral fluorophosphoranes PH_nF_{5-n} ($n = 1$, 2, 3)[4,5] and the ψ-octahedral ion PHF_5^- are known.[6] Furthermore, a range of pentacoordinated hydridosilicate anions have been prepared and characterized, for example, $SiH_2R_3^-$ and $SiH_2OR_3^-$.[7,8] Such species have received attention because of their significance as model systems, intermediates or transition states in organosilicon reactions.[9,10]

The only hypervalent all-hydrido species known so far is the ion SiH_5^- which was identified as a product of the gas phase ion–molecule reaction $Et_3SiH_2^- + SiH_4 = SiH_5^- + Et_3SiH$ by mass spectrometry.[11] This ion subsequently served as prototype for various theoretical investigations into bonding properties and the stability of hypervalent compounds.[12–15] It was found that SiH_5^- is stable with respect to the loss of H^-, but unstable with respect to decomposition into SiH_3^- and H_2.[12,15] Here we report on the thermodynamically stable solids A_2SiH_6 (A = K, Rb)—consisting of unique hypervalent all-hydrido complexes SiH_6^{2-}—which were obtained from high-pressure techniques.

Initially, a reaction $2KH + Si + 2H_2 \rightarrow K_2SiH_6$ (1) was pursued. Stoichiometric mixtures of KH and Si were pressed into a pellet which was sandwiched between two pellets of ammonia borane (BH_3NH_3). The three-pellet arrangement was then sealed in a NaCl container (inner diameter ID = 4 mm, length $l = 7.9$ mm) and exposed to high-pressure, high-temperature conditions in a multi-anvil device. At elevated temperatures, ammonia borane irreversibly decomposes to BN and $3H_2$ and thus serves as hydrogen source for the reaction.[16] Powder X-ray diffraction (PXRD) patterns of samples exposed to temperatures between 450 and 650 °C and pressures above 4 GPa revealed the formation of a face-centered cubic phase ($a \approx 7.84$ Å). However, the major part of the recovered sample (estimated at 70 %) corresponded to unreacted KH and Si. The new phase, later identified as K_2SiH_6, could be distinguished visually as greenish-yellow speckles or stripes embedded in the gray matrix of the starting material mixture. The hydridosilicate is highly sensitive to moisture. Despite numerous attempted reaction conditions (temperature, pressure, dwelling time, amount of hydrogen source, KH:Si ratio) yields for K_2SiH_6 did not significantly increase, not even when applying pressures approaching 10 GPa. As a next step the decomposition reaction $2KSi + 3H_2 \rightarrow K_2SiH_6 + Si$ (2) was considered. Although this reaction proceeded readily at pressures above 4 GPa it came at the cost of significant amounts of KBH_4 as byproduct, the boron obviously introduced by the hydrogen source BH_3NH_3. Efforts to synthesize Rb_2SiH_6 according to Equations (1) and (2) showed similar results to K_2SiH_6.

The lattice parameter a of cubic A_2SiH_6 was refined to 7.8425(9) and 8.1572(4) Å for A = K and Rb, respectively. Bragg intensities fit the K_2PtCl_6 structure type (space group $Fm\bar{3}m$) which is also adopted by A_2SiF_6. Accordingly, the structure of A_2SiH_6 corresponds to an anti-fluorite-type arrangement of SiH_6^{2-} octahedral units and alkali metal (A) cations (inset Figure 1), which are coordinated by 12 H atoms (i.e. by four tetrahedrally arranged faces from four different octahedra). The Si and A-type atoms occupy the special positions 4a (0,0,0) and 8c (1/4,1/4,1/4), respectively, while the H position 24e (x,0,0) represents the sole flexible structural parameter. This parameter cannot be reliably obtained from the refinement of PXRD patterns.

Figure 1 presents the Raman and IR spectrum of K_2SiH_6. Raman bands are observed at 1739, 1343, and 1133 cm^{-1}, and

[*] Dr. J. Nylén, Prof. U. Häussermann
Department of Materials and Environmental Chemistry
Stockholm University, 10691 Stockholm (Sweden)
E-mail: ulrich.haussermann@mmk.su.se
K. Puhakainen, S. Konar, Dr. K. Leinenweber
Department of Chemistry and Biochemistry
Arizona State University, Tempe, AZ 85287-1604 (USA)
D. Benson
Department of Physics, Arizona State University
Tempe, AZ 85287-1504 (USA)
Dr. E. Stoyanov
Peter A. Rock Thermochemistry Laboratory and NEAT ORU
University of California at Davis, Davis, CA 95616 (USA)

[**] This work was supported by the Swedish Research Council (Vetenskapsrådet) and the US National Science Foundation through grants DMR-0638826, CHE-0742006, and DMR-1007557. We gratefully acknowledge the use of facilities within the LeRoy Eyring Center for Solid State Science at Arizona State University.

Supporting information for this article is available on the WWW under http://dx.doi.org/10.1002/anie.201108713.

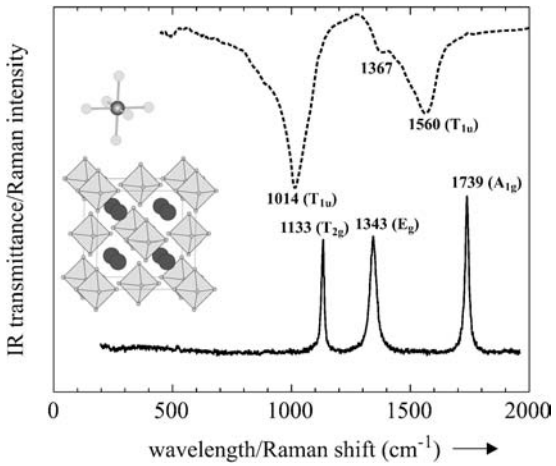

Figure 1. Raman (lower curve) and IR spectrum (upper curve) of K_2SiH_6. Bands correspond to Si–H stretching and bending modes and are assigned assuming SiH_6^{2-} entities with O_h symmetry. The unassigned band at 1367 cm^{-1} may be from an impurity or a result of Fermi resonance. Inset shows an octahedral SiH_6^{2-} entity (Si: medium gray, H: light gray) and their arrangement in the cubic face-centered K_2SiH_6 structure (K: dark gray)

two major IR bands appear at 1560 and 1014 cm^{-1}. An octahedral ion SiH_6^{2-} will give rise to six internal fundamental modes, three Si–H stretches with symmetry A_{1g} (R), E_g (R), and T_{1u} (IR) and three Si–H bends with symmetry T_{2g} (R), T_{1u} (IR), and T_{2u} (ia). Activities are specified in parenthesis (IR = IR-active, R = Raman-active, ia = inactive). This agrees with the number of observed bands, and we assign the bands at 1739, 1560, and 1343 cm^{-1} as Si–H stretches and those at 1133 and 1014 cm^{-1} as Si–H bends. We note that the frequencies of the stretching modes appear considerably decreased in comparison with normal-valent tetrahedral silane SiH_4 ($\tilde{\nu}_1(A_1) = 2186$ cm^{-1}, $\tilde{\nu}_3(T_2) = 2189$ cm^{-1}), while the bends are at slightly higher frequencies (SiH_4: $\tilde{\nu}_2(E) = 972$ cm^{-1}, $\tilde{\nu}_4(T_2) = 913$ cm^{-1}).[17] On the other hand, for $Ph_3SiH_2^-$ the IR frequency of Si–H was observed at 1524 cm^{-1}, which would be in reasonable agreement with the finding for SiH_6^{2-}.[8b] In $Ph_3SiH_2^-$ hydrogen takes the axial (3c4e bonded) positions in the trigonal bipyramidal ligand environment.[8a]

First-principles calculations have been employed to analyze electronic structure, chemical bonding, and thermodynamic stability of K_2SiH_6. The computational optimization of the K_2SiH_6 structure yielded a lattice parameter 7.852 Å (7.978 Å when more realistically considering the effect of zero-point energy (ZPE) to the equilibrium volume) which is in close agreement with the experimental value. The H positional parameter was obtained as $x = 0.2058$ which resulted in a Si–H distance of 1.62 Å (not changed when ZPE corrected). This distance compares favorably to $R_3SiH_2^-$ where the two Si–H distances have been reported as 1.64 and 1.65 Å[8a] and to the axial distance in SiH_5^- in its computed equilibrium structure (1.61–1.64 Å).[12,15]

The electronic band structure of K_2SiH_6 is shown in Figure 2a and compared to the archetypical hypervalent system K_2SiF_6. The occupied bands for K_2SiH_6 mirror the molecular orbital energy levels of SiH_6^{2-}. The highest lying e_g-type band, which is nonbonding and primarily composed of H states, shows a significant dispersion (about 1.5 eV). The calculated band gap has a size of about 2 eV and is indirect

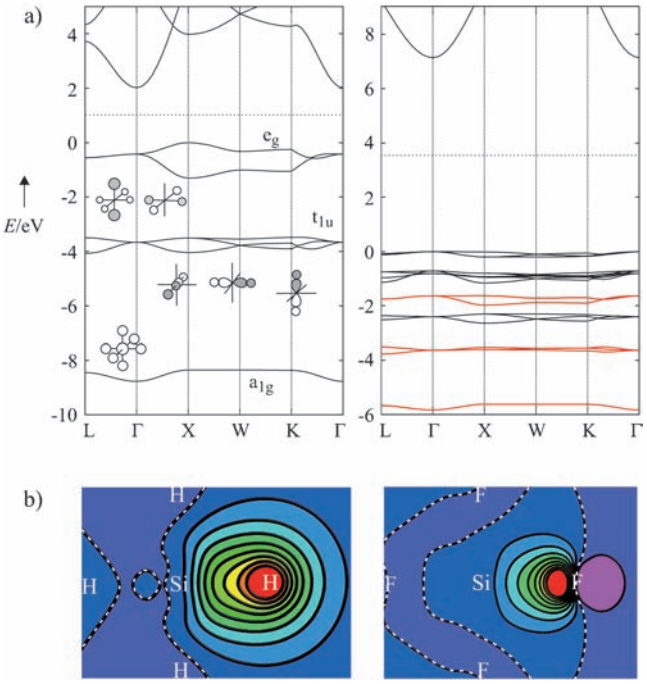

Figure 2. a) Band structures of K_2SiH_6 (left) and K_2SiF_6 (right). The horizontal dotted line corresponds to the center of the bandgap. Inset represents the molecular orbitals of the hypervalent bond in SiH_6^{2-}. Bands accounting for hypervalent bonding in K_2SiF_6 are highlighted in red. b) Contour maps of maximally localized Wannier functions associated with a Si–H (left) and a Si–F bond (right) in K_2SiH_6 and K_2SiF_6, respectively. The broken white line separates positive from negative values.

due to the dispersion behavior of the e_g band. In contrast, because of the electronegative F ligands, K_2SiF_6 (a = 8.3044 Å, $d_{Si\text{-}F} = 1.72$ Å)[18] attains a wide band gap (with a size of about 7 eV). The occupied bands are considerably less dispersed compared to K_2SiH_6. The nonbonding e_g band is embedded between bands accounting for lone pair states, and because of the altered nature of the highest occupied band the band gap is direct.

The rather different nature of the hypervalent Si–H bond compared to Si–F is highlighted by their maximally localized Wannier functions (MLWFs), as shown in Figure 2b. Generally, the Wannier representation allows a real-space presentation of the electronic structure based on localized orbitals.[19] However, Wannier functions are constructed from extended Bloch states and are non-unique. Marzari and Vanderbilt developed a procedure to iteratively minimize the spread of the Wannier functions so that they are well localized about their centers, hence MLWFs.[20] The calculation for K_2SiH_6 yields six spatially separated and equivalent MLWFs corresponding to Si–H bond orbitals. In addition to Si–F bond orbitals, for K_2SiF_6 MLWFs corresponding to lone pairs around F are also obtained. Both Si–H and Si–F MLWFs are centered at the electronegative atom; however

their spread, that is, the measure of localization, is rather different: 1.201 Å^2 for Si–H and 0.438 Å^2 for Si–F. This means that the Si–F MLWF is considerably more localized. As a matter of fact, the spread for the Si–F MLWF is essentially the same as for the lone pair MLWF (0.436 Å^2), which underlines the very high polarity of the Si–F bond.

The different ionicities of K_2SiH_6 and K_2SiF_6 may be quantified through a Bader analysis which partitions the total electron density distribution in the unit cell into atomic regions, defined as surfaces through which the gradient of the density has zero flux.[21] By integrating the charge density within a region associated to a nucleus the total charge on an atom can be uniquely estimated. The results are compiled in Table 1. KH and KF with the NaCl structure are included as reference systems. As expected, the charge transfer in KF (±0.86) is considerably larger than in KH (±0.76), manifesting the higher ionicity of the former. Interestingly, F in K_2SiF_6 attains a very similar

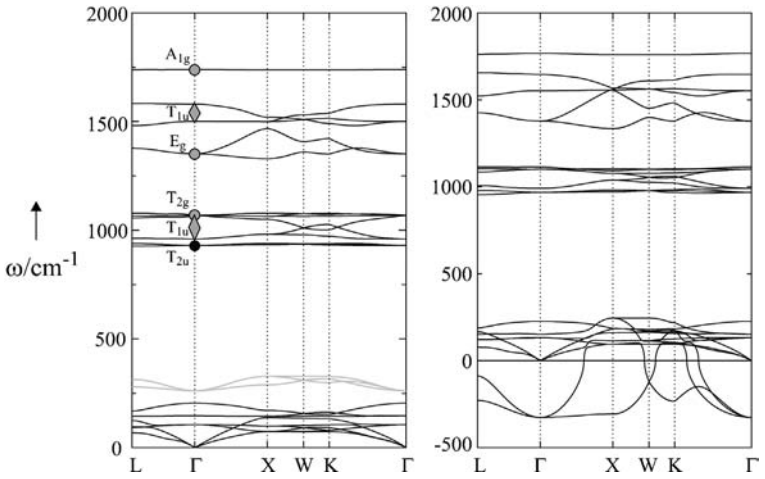

Figure 3. Left: Calculated phonon dispersion curves for K_2SiH_6 at the ZPE equilibrium volume. Gray circles mark the Raman-active modes, diamonds the LO–TO split IR-active modes, and the black circle the inactive mode. The phonon dispersion of the libration mode is indicated as gray lines. Right: Corresponding phonon dispersion curve for Na_2SiH_6. Frequencies of the libration mode are imaginary.

Table 1: Atomic charges according to a Bader analysis.[21]

KH	K	+0.760	KF	K	+0.857
	H	−0.760		F	−0.857
K_2SiH_6	K	+0.809	K_2SiF_6	K	+0.912
	Si	+2.502		Si	+3.251
	H	−0.687		F	−0.846

charge to F in KF (−0.85) which in turn yields high positive charges for Si and K (+3.25 and +0.91, respectively). This indicates that highly electronegative F determines the ionicity of K_2SiF_6. In contrast, the charge for H in K_2SiH_6 is considerably lower (−0.69) compared to H in KH, leading to less positive charges on Si and K (+2.50 and +0.81, respectively).

First-principles calculations of phonons (within the quasi-harmonic approximation) provide the possibility to confirm the assignment of experimentally determined vibrational modes (Figure 1), investigate the dynamical stability of compounds, and assess thermodynamic functions.[22] Figure 3 a (left) shows the calculated phonon dispersion relations for K_2SiH_6 at the computed (theoretical) ZPE volume. These dispersion curves show the phonon frequencies along special directions in the Brillouin zone (BZ); k points describe the propagation direction and the modulation of displacements of a phonon. Inelastic neutron scattering allows the experimental determination of phonon dispersions, the situation at the zone center (Γ point) is accessible by optical spectroscopy (IR and Raman).

The mode with the highest frequencies has virtually no dispersion and corresponds to the Raman-active total symmetric stretch A_{1g} at Γ. The calculated frequency at Γ (1739 cm^{-1}) is in excellent agreement with experiment (1739 cm^{-1}, cf. Figure 1). The next modes show dispersion and relate to the IR-active T_{1u} mode, which is split at the Γ point (LO–TO splitting), and the Raman-active E_g mode. The T_{1u} components have the frequencies 1580 cm^{-1} (TO) and 1501 cm^{-1} (LO), and the E_g mode has 1352 cm^{-1}. This is again in perfect agreement with experiment (1560 and 1343 cm^{-1}, respectively). Modes associated with bends are located around 1000 cm^{-1}, the Raman-active T_{2g} mode is calculated at 1069 cm^{-1}, the components of IR-active T_{1u} are at 1067 cm^{-1} (TO) and 959 cm^{-1} (LO), and the inactive T_{2u} mode is at 930 cm^{-1}. For the bends calculated frequencies seem underestimated by about 6 % compared to experiment.

The internal modes (arising from the entities SiH_6^{2-}) are clearly separated from the external (lattice) modes and appear below 500 cm^{-1}. Lowest in frequency are the acoustic and the two optic translation modes T_{2g} and T_{1u} (K^+ vibrates against SiH_6^{2-}). The libration (or torsion) mode is dispersed around 300 cm^{-1}. Libration describes the rotation of octahedral units against each other and involves only hydrogen motion. The phonon dispersion of this mode is highlighted in Figure 3 (left). The mode is inactive in optical spectroscopy (T_{1g}) but may be involved in a combination with the also inactive T_{2u} bend and thus give rise to Fermi resonance,[23] which could explain the feature in the IR spectrum at 1367 cm^{-1} (Figure 1). Interestingly, libration appears to determine dynamical stability of hydridosilicates A_2SiH_6. Figure 3 (right) shows the phonon dispersion relation for hypothetical Na_2SiH_6. At the theoretical equilibrium volume phonon frequencies of the libration mode are imaginary throughout most of the BZ, meaning that this mode is instable and thus Na_2SiH_6 with the K_2PtCl_6 structure is not accessible. The reason is probably that dynamical stability of hydridosilicates A_2SiH_6 requires a sufficient separation of SiH_6^{2-} octahedra in the structure, which is not possible with smaller alkali metals.

The application of high pressure for the synthesis of K_2SiH_6 may raise the suspicion that the compound represents a metastable high-pressure phase. With knowledge of the phonon density of states the vibrational contributions to internal energy *E* (that includes ZPE), entropy *S*, and

Helmholtz free energy F can be computed.[24] In the quasiharmonic approximation phonons are harmonic but volume-dependent. The equilibrium volume of a system is established by minimizing $F_{(T)}$. The difference of the Gibbs free energy for the formation reaction $2\,KH + Si + 2\,H_2 \rightarrow K_2SiH_6$ is $\Delta G_{(T)} = G_{(T)}[K_2SiH_6] - 2\,G_{(T)}[KH] - G_{(T)}[Si] - 2\,G_{(T)}[H_2]$ with $G_{(T)} = H_{(T)} - TS_{(T)}$. The temperature-dependent contribution to the Gibbs free energy for a hydrogen molecule was approximated by using values for $H_{(T)}$, $S_{(T)}$, and $H_{(0)}$ from thermochemical tables.[25]

The result is shown in Figure 4 and decomposed into ΔH and $T\Delta S$ terms. The enthalpy difference $\Delta H_{(T)}$ is negative and its values are slightly decreasing with increasing temperature.

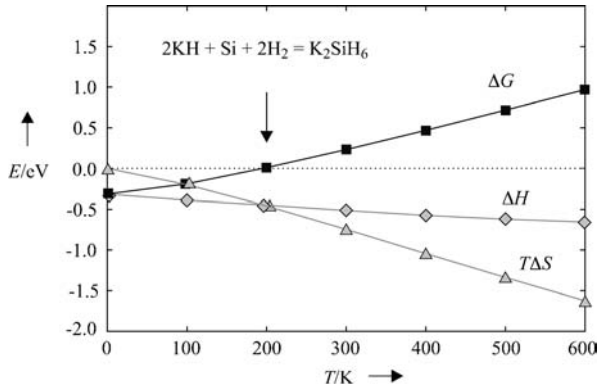

Figure 4. Temperature-dependent energy differences between [2 KH + Si + 2 H_2] and K_2SiH_6. ΔG, $T\Delta S$, and ΔH denote the difference in Gibbs free energy, in entropy contribution, and in enthalpy, respectively. The calculated decomposition temperature of K_2SiH_6 is marked with an arrow.

Thus the formation reaction is exothermic. The $T\Delta S$ term is always negative and follows largely that of a hydrogen molecule, $T\Delta S_{(T)}[H_2]$.[24] At about 200 K $T\Delta S$ equals ΔH. At higher temperatures K_2SiH_6 is unstable with respect to KH, Si, and H_2 and will decompose if not prevented for kinetic reasons. The stability of Rb_2SiH_6 is calculated slightly higher, at 260 K. The significance of pressure for the synthesis of A_2SiH_6 (A = K, Rb) is two-fold. Firstly, with pressure the decomposition temperature will shift to higher values, thus enabling the application of elevated temperature for synthesis. Secondly, at pressures above 1 GPa the activity of molecular hydrogen increases sharply, which favors hydridosilicate formation.[26]

In conclusion, we have shown that high-pressure synthesis affords elusive all-hydrido hypervalent species, namely octahedral complexes SiH_6^{2-} in the crystalline hydridosilicates A_2SiH_6 (A = K, Rb). The compounds seem weakly stable with respect to decomposition into AH, Si, and H_2. Stability increases with increasing size of A, which is equivalent with a larger separation of SiH_6^{2-} entities. For lighter alkali metals (e.g. Na) A_2SiH_6 is dynamically unstable. With H as a ligand the hypervalent bond attains a peculiar, relatively weakly polar, character. As a consequence, occupied nonbonding molecular orbitals accompanying the hypervalent bond are high in energy, which results in a small HOMO–LUMO (band) gap compared to traditional hypervalent systems with electronegative ligands. Compared to normal valent silanes the Si–H bond length in SiH_6^{2-} appears considerably enlarged, by about 0.15 Å. Accordingly, Si–H stretching frequencies are drastically reduced, by about 400–500 cm^{-1}, reflecting the weakness of a hypervalent Si–H bond.

Experimental Section and Methods

In a typical synthesis 50–70 mg of a mixture of AH/Si or ASi were sealed in a NaCl capsule together with ammonia borane as a hydrogen source (20 mg, Si:H ratio at least 1:10). The capsules were compressed in a multi-anvil device[27] to a pressure between 4 and 9 GPa and subsequently heated to a temperature between 400 and 700 °C at a rate of 1–2 °C min^{-1}. Depending on the applied pressure ammonia borane decomposes between 200 and 320 °C to BN and H_2.[16] After equilibrating samples at their target temperature for 1 h, the temperature was quenched and the pressure released at a rate of approximately 0.5 GPa h^{-1}. The preparation of sample capsules and their recovery after high pressure, high temperature treatment was performed in an Ar filled glove box. The procedure of multi-anvil gigapascal hydrogenation using ammonia borane as internal hydrogen source has been described in detail in Ref. [28].

Products were analyzed by powder X-ray diffraction (PXRD), Raman and IR spectroscopy. Samples were ground, loaded into 0.3 mm capillaries, and measured on a Bruker D8 Advance diffractometer ($Cu_{K\alpha}$ radiation). Lattice parameters were obtained from Rietveld refinement as well as least-squares refinement of the measured and indexed lines.[29,30] Raman spectra were recorded on capillary sealed samples that were also used for PXRD. A custom built system was employed using a frequency-doubled YAG laser at 532 nm as excitation source and a liquid nitrogen cooled CCD detector. IR spectroscopy was carried out on a Bruker IFS 66v/s instrument. KBr pellets were prepared in a glove box and transferred in a closed container to the spectrometer.

Calculations were performed in the framework of the frozen core all-electron Projected Augmented Wave (PAW) method,[31] as implemented in the program VASP,[32] and the plane wave Abinit code[33] employing the GGA-PBE as the exchange correlation.[34] Si, H, and F pseudopotentials were obtained from the fhi98PP package.[35] For K and Rb the pseudopotentials according to Goedecker, Teter, and Hutter were used.[36]

The Supporting Information contains further details on the synthesis procedure, the analysis of products (including Rb_2SiH_6), and the computational procedure.

Received: December 10, 2011
Published online: February 9, 2012

Keywords: coordination chemistry · high-pressure hydrogenation · hydrido complexes · hypervalent silicon · multi-anvil technique

[1] S. Noury, B. Silvi, R. Gillespie, *Inorg. Chem.* **2002**, *41*, 2164–2172.
[2] a) R. J. Hach, R. E. Rundle, *J. Am. Chem. Soc.* **1951**, *73*, 7940–7951; b) G. C. Pimentel, *J. Chem. Phys.* **1951**, *19*, 446–446; c) V. B. Koutecky, J. I. Musher, *Theor. Chim. Acta* **1974**, *33*, 227–238.
[3] "Hypervalent compounds": G. S. McGrady, J. W. Steed in *Encyclopedia of Inorganic Chemistry 2* (Ed.: R. B. King), Wiley, Chichester, **2005**, p. 1938.
[4] P. M. Treichel, R. A. Goodrich, S. B. Pierce, *J. Am. Chem. Soc.* **1967**, *89*, 2017–2022.

[5] a) F. Seel, K. Vellemann, *Z. Anorg. Allg. Chem.* **1971**, *385*, 123 – 130; b) H. Beckers, *Z. Anorg. Allg. Chem.* **1993**, *619*, 1869 – 1879.

[6] a) K. O. Christe, D. A. Dixon, W. W. Wilson, *J. Am. Chem. Soc.* **1994**, *116*, 7123 – 7128; b) R. Minkwitz, S. Schneider, A. Kornath, *Inorg. Chem.* **1998**, *37*, 4662 – 4665.

[7] a) R. J. P. Corriu, C. Guerin, B. J. L. Henner, Q. Wang, *Organometallics* **1991**, *10*, 3574 – 3581; b) R. Corriu, C. Guerin, B. Henner, Q. Wang, *Inorg. Chim. Acta* **1992**, *198 – 200*, 705 – 713.

[8] a) M. J. Bearpark, G. S. McGrady, P. D. Prince, J. W. Steed, *J. Am. Chem. Soc.* **2001**, *123*, 7736 – 7737; b) P. D. Prince, M. J. Bearpark, G. S. McGrady, J. W. Steed, *Dalton Trans.* **2008**, 271 – 282.

[9] C. Chuit, R. J. P. Corriu, C. Reye, J. C. Young, *Chem. Rev.* **1993**, *93*, 1371 – 1448.

[10] A. P. Bento, F. M. Bickelhaupt, *J. Org. Chem.* **2007**, *72*, 2201 – 2207.

[11] D. J. Hajdasz, R. R. Squires, *J. Am. Chem. Soc.* **1986**, *108*, 3139 – 3140.

[12] T. Taketsugu, M. S. Gordon, *J. Phys. Chem.* **1995**, *99*, 14597 – 14605.

[13] J. Moc, *J. Mol. Struct.* **1999**, *461/462*, 249 – 259, and references therein.

[14] E. P. A. Couzijn, A. W. Ehlers, M. Schakel, K. Lammertsma, *J. Am. Chem. Soc.* **2006**, *128*, 13634 – 13639.

[15] a) S. C. A. H. Pierrefixe, F. M. Bickelhaupt, *Struct. Chem.* **2007**, *18*, 813 – 819; b) S. C. A. H. Pierrefixe, C. F. Guerra, F. M. Bickelhaupt, *Chem. Eur. J.* **2008**, *14*, 819 – 828.

[16] J. Nylén, T. Sato, E. Soignard, J. L. Yarger, E. Stoyanov, U. Häussermann, *J. Chem. Phys.* **2009**, *131*, 104506.

[17] a) K. Ohno, H. Matsuura, Y. Endo, E. Hirota, *J. Mol. Spectrosc.* **1985**, *111*, 73 – 82; b) W. D. Allen, H. F. Schaefer III, *Chem. Phys.* **1986**, *108*, 243 – 274.

[18] The experimental values are $a = 8.134(1)$ and $d(\mathrm{Si{-}F}) = 1.683(1)$ Å (J. Loehlin, *Acta Crystallogr. Sect. C* **1984**, *40*, 570).

[19] G. H. Wannier, *Phys. Rev.* **1937**, *52*, 191 – 197.

[20] N. Marzari, D. Vanderbilt, *Phys. Rev. B* **1997**, *56*, 12847 – 12865.

[21] R. F. W. Bader, *Atoms in Molecules: A Quantum Theory*, Oxford University Press, Oxford, **1990**, pp. 1 – 52.

[22] X. Gonze, C. Lee, *Phys. Rev. B* **1997**, *55*, 10355 – 10368.

[23] S. F. Parker, *Coord. Chem. Rev.* **2010**, *254*, 215 – 234.

[24] X. Ke, I. Tanaka, *Phys. Rev. B* **2005**, *71*, 024117.

[25] M. W. Chase, Jr., C. A. Davies, J. R. Downey Jr., D. J. Frurip, R. A. McDonald, A. N. Syverud, *NIST–JANAF Thermochemical Tables*, National Institute of Standards and Technology, Gaithersburg, **1985**.

[26] a) H. Hemmes, A. Driessen, R. J. Griessen, *Phys. C* **1986**, *19*, 3571 – 3585; b) A. Driessen, P. Sänger, H. Hemmes, R. Griessen, *J. Phys. Condens. Matter* **1990**, *2*, 9797 – 9814; c) Y. Fukai, *J. Alloys Compd.* **2005**, *404/405*, 7 – 15.

[27] E. Stoyanov, U. Häussermann, K. Leinenweber, *High Pressure Res.* **2010**, *30*, 175 – 189.

[28] K. Puhakainen, E. Stoyanov, M. J. Evans, K. Leinenweber, U. Häussermann, *J. Solid State Chem.* **2010**, *183*, 1785 – 1789.

[29] A. X. S. Bruker, TOPAS V4: General Profile and Structure Analysis Software for Powder Diffraction Data, User's Manual, Karlsruhe, Germany, **2008**.

[30] P.-E. Werner, *Ark. Kemi* **1969**, *31*, 513 – 516.

[31] a) P. E. Blöchl, *Phys. Rev. B* **1994**, *50*, 17953 – 17979; b) G. Kresse, J. Joubert, *Phys. Rev. B* **1999**, *59*, 1758 – 1775.

[32] a) G. Kresse, J. Hafner, *Phys. Rev. B* **1993**, *48*, 13115 – 13118; b) G. Kresse, J. Furthmüller, *Comput. Mater. Sci.* **1996**, *6*, 15 – 50.

[33] X. Gonze, B. Amadond, P. M. Anglade, J. M. Beuken, F. Bottin, P. Boulanger, F. Bruneval, D. Caliste, R. Caracas, M. Côté, T. Deutsch, L. Genovese, Ph. Ghosez, M. Giantomassi, S. Goedecker, D. R. Hamann, P. Hermet, F. Jollet, G. Jomard, S. Leroux, M. Mancini, S. Mazevet, M. J. T. Oliveira, G. Onida, Y. Pouillon, T. Rangel, G. M. Rignanese, D. Sangalli, R. Shaltaf, M. Torrent, M. J. Verstraete, G. Zerah, J. W. Zwanziger, *Comput. Phys. Commun.* **2009**, *180*, 2582 – 2615.

[34] J. P. Perdew, K. Burke, M. Ernzerhof, *Phys. Rev. Lett.* **1996**, *77*, 3865 – 3868.

[35] M. Fuchs, M. Scheffler, *Comput. Phys. Commun.* **1999**, *119*, 67 – 98.

[36] a) S. Goedecker, M. Teter, J. Hutter, *Phys. Rev. B* **1996**, *54*, 1703 – 1710; b) C. Hartwigsen, S. Goedecker, J. Hutter, *Phys. Rev. B* **1998**, *58*, 3641 – 3662; c) M. Krack, *Theor. Chem. Acc.* **2005**, *114*, 145 – 152.

